

CONF-761125--1

TITLE: GLOBAL SEISMIC EFFECTS OF BASIN-FORMING IMPACTS


AUTHOR(S): H. Grady Hughes, J-DOT, LASL
Fred N. App, J-9, LASL
Thomas R. McGetchin, G-6, LASL

SUBMITTED TO: Proceedings of the Conference on Comparisons
of Mercury and the Moon, November 1976
The Lunar Science Institute
3303 NASA Road 1
Houston, Texas 77058

NOTICE
This report was prepared as an account of work sponsored by the United States Government. Neither the United States nor the United States Energy Research and Development Administration, nor any of their employees, nor any of their contractors, subcontractors, or their employees, makes any warranty, express or implied, or assumes any legal liability or responsibility for the accuracy, completeness or usefulness of any information, apparatus, product or process disclosed, or represents that its use would not infringe privately owned rights.

By acceptance of this article for publication, the publisher recognizes the Government's (license) rights in any copyright and the Government and its authorized representatives have unrestricted right to reproduce in whole or in part said article under any copyright secured by the publisher.

The Los Alamos Scientific Laboratory requests that the publisher identify this article as work performed under the auspices of the USERDA.


los alamos
scientific laboratory
of the University of California
LOS ALAMOS, NEW MEXICO 87545

An Affirmative Action/Equal Opportunity Employer

MASTER

DISTRIBUTION OF THIS DOCUMENT IS UNLIMITED

ABSTRACT

NOTICE
This report was prepared as an account of work sponsored by the United States Government. Neither the United States nor the United States Atomic Energy Commission, nor any of their employees, nor any of their contractors, subcontractors, or their employees, make any warranty, express or implied, or assume any legal liability or responsibility for the accuracy, completeness or usefulness of any information, apparatus, product or process disclosed, or represent that its use would not infringe privately owned rights.

Models of the thermal evolution of the moon and the terrestrial planets suggest that basin-forming impacts occurred when the planets had partially molten interiors overlain by thickening lithospheres, comparable in thickness to the basin radii. We are investigating the effects of large impacts on planetary surfaces using a Lagrangian computer program which treats shock wave propagation and includes the effects of material strength, elastic-plastic behavior and material failure. In this paper we describe the computer code and some physical details of our numerical techniques, and report the results of several initial calculations. We study the global seismic effects for cratering energies (10^{24} and 10^{25} J) intermediate between the Copernicus and Imbrium events on the moon, and compare the phenomenologies for assumed solid and molten planetary interiors. The principal results are as follows: 1) Far-field effects are largely independent of cratering mechanisms (e.g., simulated impact vs buried explosion). 2) Antipodal seismic effects are significantly enhanced by focusing and are of substantial magnitude. Vertical ground motion may be on the order of kilometers, and accelerations approach one lunar-g. 3) The most violent activity occurs at significant depth beneath the antipode, considerably after the passage of the initial compressive/rarefactive shock wave, and results from

complex interactions with the free surface. 4) Seismic effects are decidedly more pronounced for a molten planet than for a solid one. 5) Tensile failure may occur at depths of tens of kilometers beneath the antipode, and may also occur over the entire surface, although at shallower depths.

These results support the suggestion of Schultz and Gault (1975 a,b) that the unusual terrains antipodal to large planetary basins may have been catastrophically modified by seismicity generated by the basin-forming impacts. We would further suggest that these impacts may in fact have pervasively and repeatedly brecciated the entire lithospheres of the terrestrial planets as these lithospheres formed and thickened.

1. Introduction

Crater structure, distribution of ejecta and seismic effects of large impacts are closely related problems of great interest in lunar and planetary science. Very large circular basins are known to exist on each of the terrestrial planets and the moon. The events which formed these structures are important elements in the historical evolution of the crusts of these planets.

Work on the lunar basins has focused on their significance as source areas for material which blankets the highlands - a sort of sandwich of ejecta units deposited in sequence from the several large basins. There is much interest and considerable disagreement regarding the thickness of these deposits. The debate centers on the volume of material excavated by the impacts which formed them. One particularly important aspect of this argument concerns the depth to which the large impacts sample the underlying layers, hence bears directly on the question of evaluating which of the lunar samples returned by Apollo may have deep-seated origins, such as the dunite (72415) and norite (78235) from the Apollo 17 site. The geometry of the basins, the thickness of the basaltic mare-fill, the relationship of the radius of the crater of excavation to the present topographic expression (which includes possible large-scale slump) all relate directly to crater-formation mechanics.

. The sequence and brief time span involved in the formation of the lunar basins is in part responsible for the view that early heating of the outer parts of the moon was caused by intense particle flux. This release of gravitational potential energy is one means of supplying heat required for extensive melting of the outer layers, sometimes referred to as the lunar magma ocean. Most currently popular models of the thermal evolution of the moon and terrestrial planets embody such a view. In these models, as time passes, the early lithosphere thickens and the interior molten layer shrinks, until at about 2 b.y. (for the small planets - Moon, Mercury, and Mars) crystallization is complete. It was during this early partly molten phase of lunar history that the large impact basins were formed and the mare basalts erupted. The large basins on Mercury and Mars presumably were formed in a similar way. These basin-forming impacts appear to have occurred at a time when the ratio of lithospheric thickness to crater diameter was small, perhaps less than unity. Hence, the large impacts penetrated and fragmented the lithosphere, much as an explosive charge would disrupt the surface of an ice-covered but only partially frozen lake.

Prominent among previous workers who have addressed themselves to the process of large impact basin formation are Shoemaker and Hackman (1962), Stuart-Alexander and Howard (1970), Wilhelms and McCauley (1971), Hartmann and Wood (1971), McGetchin et al (1973), Pike (1974), Head (1974), Head et al

(1975), and recently by computer methods, O'Keefe and Ahrens (1975). Stated in general terms, the problem is to assess the effects of large impacts on layered, partially molten planets. We wish to understand the details of the crater formation history and distribution of ejecta, post-crater deformation processes, and associated seismic disturbances.

The observations and prior results which most directly motivated us are described in papers by Gault and Wedekind (1969), Schultz (1972, 1974), and Schultz and Gault (1975a, 1975b). Gault and Wedekind fired small projectiles at glass spheres of tektite composition and observed both large craters and large spallation zones antipodal to the craters. Schultz ascribed the origin of the hilly and grooved terrains antipodal to the major lunar basins Imbrium and Orientale, and to the Caloris basin on Mercury, to the effects of focused impact-generated body and surface waves. Schultz and Gault show that for the Orientale event a body wave arrives at the antipode about 8 minutes after an impact; ejecta is dispersed in time between about 28 and 50 minutes; and surface waves arrive later yet, some 80 minutes after impact. These results certainly are dependent on both the conditions and scale of the impact and also importantly on the physical properties and structural configuration of the planetary interior. We wish to extend the work of Schultz and Gault (1975 a,b), namely to describe quantitatively and in detail the seismic effects of the very large impacts; eventually

to parameterize certain aspects of impact energy, internal structure (such as the thickness and depth of the molten layer), and physical properties; and to examine the results in light of potentially observable effects on geological features. This paper presents our methods and some initial results.

The plan of the paper is as follows. In Section 2 we present the essentials of the numerical methods which we employ. Since these techniques have not received extensive discussion in the planetary sciences literature, we have chosen to include a fairly detailed description of our general computational approach. In Section 3 we discuss specific methods used in the present work and describe the results of selected calculations. Section 4 presents conclusions and some possible planetological implications.

2. A Computational Tool for Impact Studies

The TOODY3 Lagrangian finite difference computer program (Bertholf and Benzley, 1968) calculates solutions to wave propagation problems in two dimensions. TOODY3 employs either a rectangular coordinate system, with one direction being a direction of translational symmetry along which strains vanish, or a cylindrical system, with one axis being an axis of rotational symmetry. Figure (1b) illustrates one of the computational meshes used in this study. Here the horizontal axis is the symmetry axis, and the planet thus represented is spherical.

The term Lagrangian applies to a computational mesh which moves with the material, so that no mass is transferred between zones of the mesh. The price one pays for this lack of diffusion is an eventually severe distortion of the mesh, which if left uncorrected would destroy the accuracy of the finite difference method. TOODY3 is therefore used in combination with an automatic rezoning program called TOOREZ (Thorne and Holdridge, 1974) which intermittently realigns the distorted mesh into a near-orthogonal configuration. Some diffusion is of course introduced when the rezoner is used, but on the whole, this intermittently rezoned Lagrangian procedure appears to be less diffusive than Eulerian or continuously rezoned Lagrangian methods.

TOODY3 approximates a description of the state of a large system by specifying the values of the thermodynamic and structural variables at a finite number of points of the

system (the computational mesh). Given the state of the system at a time t , the program predicts the state at the subsequent time $t + \delta t$. This cycle is repeated as often as needed to calculate the evolution of the system in time.

Figure (2) depicts the logical path followed in advancing the calculation by one time step. Given the initial stress field, the acceleration \vec{a} of the material in each zone is computed from equations which are equivalent to the conservation of momentum. In cylindrical coordinates, with rotational symmetry about the z -axis, these equations are

$$-\rho(a^x - g^x) = \delta T^{xx}/\delta x + \delta T^{xz}/\delta z + (T^{xx} - T^{zz})/x, \quad (1a)$$

$$-\rho(a^z - g^z) = \delta T^{xz}/\delta x + \delta T^{zz}/\delta z + T^{xz}/x. \quad (1b)$$

Here x and z are the (cylindrically) radial and axial coordinates, respectively; ρ is the material density; \vec{g} is the acceleration due to gravity; and T^{xx} , T^{zz} , and T^{xz} are respectively the radial, axial, and shear stresses. For the sake of clarity we have omitted viscous terms which also enter equations (1).

Once the accelerations are known, velocities u^x , u^z and displacements δx , δz are calculated from the obvious kinematical formulae

$$a^x = \delta u^x / \delta t, \quad a^z = \delta u^z / \delta t, \quad (2a)$$

$$u^x = \delta x / \delta t, \quad u^z = \delta z / \delta t. \quad (2b)$$

The local strain rates d^{ij} are then calculated from

$$d^{xx} = \delta u^x / \delta x, \quad d^{zz} = \delta u^z / \delta z, \quad (3a)$$

$$d^{xz} = d^{zx} = 1/2(\delta u^x / \delta z + \delta u^z / \delta x), \quad (3b)$$

$$d^{\theta\theta} = u^x / x, \quad (3c)$$

and the resulting updated strains give rise to the new stress field via a set of equations of state. The logical loop of Figure (2) is then complete, and the time-incremented stress field known.

The present version of the TOODY3 code includes several different models for the equations of state. We shall discuss only the one used in the sample calculations presented in the next section. We require of the equations of state the following properties:

- 1) Variable shear and bulk moduli which can be chosen to match experimental data or theoretical models of planetary interiors.
- 2) A shear strength which may be dependent on pressure, decreases with increasing temperature, and is zero in the molten state.
- 3) Realistic models of shear and tensile failure.
- 4) Realistic descriptions of melting and vaporization.

We first list the various parameters which enter our constitutive equations:

- ρ = material density
- ρ_0 = density in the cold unstressed state
- η = compression = $1 - \rho_0/\rho$
- p = pressure = mean stress
- E = specific internal energy
- $p_H(\rho)$ = pressure along a compressive reference curve
- $E_H(\rho)$ = specific internal energy along the same reference curve

Γ_0 = Grüneisen ratio relating pressure to thermal energy

γ = ratio of specific heats in the vapor state

$H = \gamma - 1$

E_m = energy of melt

E_s = energy of sublimation

K_0 = bulk modulus in the cold unstressed state

$N = K_0(\Gamma_0 \rho_0 E_s)^{-1}$

c_0 = bulk sound speed in the cold unstressed state

For a solid compressed material, we adopt the Mie-Grüneisen equation

$$p = p_H(\rho) + \Gamma_0 \rho_0 [E - E_H(\rho)]. \quad (4)$$

The reference pressure $p_H(\rho)$ is usually an analytical fit to experimental data. We are presently using a Hugoniot relation

$$p_H = \rho_0 c_0^2 \eta (1 - s\eta)^{-2} \quad (5)$$

with one free parameter s . This form comes from the observation that for many materials the shock velocity u_s is a linear function of the particle velocity u_p :

$$u_s = c_0 + s u_p \quad (6)$$

The reference energy $E_H(\rho)$ is taken to be

$$E_H = \eta p_H (2\rho_0)^{-1} \quad (7)$$

For material with $\rho < \rho_0$ (distended or vaporized material) we use the equation

$$p = \rho \left\{ H + [\Gamma_0 - H] \sqrt{\rho/\rho_0} \right\} \left\{ E - E_s [1 - e^{N\eta(1-\eta)}] \right\} \quad (8)$$

Note that for highly expanded materials, equation (8) approaches the ideal gas law

$$p = (\gamma - 1) \rho (E - E_s) \quad . \quad (9)$$

For a material at its unstressed density ρ_0 , equation (8) reduces to

$$p = \Gamma_0 \rho_0 E \quad , \quad (10)$$

which agrees with the Mie-Grüneisen equation in the limit $\rho = \rho_0$.

It is necessary to recompute the internal energy E during each cycle. We invoke the conservation of energy to equate the rate of change of energy to the rate at which work is being done by various stresses against volume changes and distortion:

$$\rho \delta E / \delta t = P_v + P_d + Q_v + Q_d \quad . \quad (11)$$

Here P_v is the rate at which work is done by the pressure against volume changes; P_d is the rate at which work is done by deviator stresses against distortion; and Q_v , Q_d are the corresponding terms for viscous pressures and stresses. External sources of energy can also be included, but have not been written in equation (11).

In order to model shear failure and plastic flow in solid materials, we compute at each time step the second deviatoric stress invariant,

$$I_{2D} = 1/6 \left\{ (\sigma_1 - \sigma_2)^2 + (\sigma_2 - \sigma_3)^2 + (\sigma_3 - \sigma_1)^2 \right\} \quad , \quad (12)$$

in terms of the principal stresses σ_i . The von Mises criterion,

$$I_{2D} \leq Y^2/3 \quad , \quad (13)$$

then identifies the elastic shear strength of the material at each point. The strength Y may depend on density and internal energy in a variety of ways; in the present calculations we are using a simple form which allows for the softening of a heated material, and the vanishing of the shear strength in the molten state:

$$Y = Y_0 (1 - E/E_m)^2 \quad , \quad E < E_m \quad , \quad (14a)$$

$$Y = 0 \quad , \quad E > E_m \quad . \quad (14b)$$

During each cycle, stress loading is treated as an elastic process governed by the bulk modulus and Poisson's ratio (from which one finds the shear modulus). At the end of each time step the von Mises criterion (13) is examined for each point in the mesh in order to detect shear failure. If the elastic limit Y has been exceeded, the stresses at that point are returned to the yield surface along a path normal to that surface.

In a similar manner, the principal stresses are examined, and if a tension in any direction exceeds the tensile strength of the material, the stress is reduced to zero in that direction. Thereafter the material is considered fractured at that location, and its tensile strength is set to zero.

We shall forgo a discussion of the finite difference equations, artificial viscosity, numerical stability, and

other matters primarily of concern to numerical hydro-dynamicists. The interested reader may find an excellent introductory treatment of these topics, together with references to more advanced works, in Harlow and Amsden (1971). This therefore concludes our description of our of our general computational methods.

3. Sample Calculations

In this section we will describe some of the specific techniques which we have developed to study the global effects of impacts. We have shown in Figure (1) a typical computational mesh representing a spherical planet. It is necessary to establish for each zone of the mesh appropriate initial values of the thermodynamic and structural variables corresponding to the static equilibrium configuration of the planet, and then to simulate the impact event in a suitable manner. To this end we select a density profile $\rho(r)$, where r is the (spherically) radial distance from the center of the planet to a given interior point. This density profile may be taken from a theoretical planetary model which we wish to investigate, or it may be computed as a solution to the equation of hydrostatic equilibrium for a given equation of state. Having selected $\rho(r)$ we assign to each zone of the mesh an appropriate pressure $p(r)$ and internal energy density $E(r)$, and to each vertex a gravitational acceleration $\vec{g}(\vec{r})$ in such a way that these quantities are all consistent with the equation of state and with the finite difference form of the equation of hydrostatic equilibrium

$$\vec{g} = -\vec{\nabla}p, \quad (15a)$$

$$|g| = G r^{-2} \int_0^r 4\pi s^2 \rho(s) ds. \quad (15b)$$

The gravitational field is not recomputed during the calculation of the impact event. Thus in regions of large material motions (i.e. near the impact point) an error will be introduced, especially for the crater ejecta. However in

the present study we are interested in the regions far from the impact, and particularly in the antipodal point. In these regions little bulk motion of the material occurs, and the gravitational field computed by (15) remains a good approximation. Furthermore, as we shall soon see, the behavior of the far-field shock waves is very little affected by the details of the energy release and crater formation.

The most important effect of the gravitational field on seismicity is to provide throughout the planetary interior an ambient overburden (hydrostatic pressure) which is usually greater than the strength of the impact-generated shock wave. It follows that throughout most of the planet, the behavior of the shock wave is insensitive to the tensile strength of the material. The reason is clear: in order to approach the tensile limit of the material, a rarefactive wave must first overcome the compressive overburden. This overburden increases rapidly with increasing depth in the planet, but the strength of the shock wave decreases rapidly as it travels away from its source. Thus the material tends to remain compressed, even when transmitting a rarefactive wave. This convenient masking of an ill-known material property does not occur for shear strength, a parameter to which the calculation is quite sensitive. We shall return shortly to this point.

We now turn to the impact itself. In most of our calculations we have, for the convenience of the computer, simulated an impact by depositing the proper amount of internal energy into one mesh zone near the surface of the planet.

This procedure models the impact as a buried explosion, a situation in which it is well known that cratering phenomenology is very sensitive to the manner of energy deposition, specifically to the scaled depth of burst for buried explosives. By contrast the global seismic disturbance is quite insensitive to the mode of energy release. To illustrate this insensitivity, we present in Figure (3) a comparison between an impact and a buried explosion of approximately the same energy ($\approx 10^{24}$ J). These figures are contour plots of the second deviatoric stress invariant, defined by equation (12), which represents essentially the distortion of the material. They show the general configuration of the internal shearing stresses at a time when the leading edge of the initial shock wave has almost reached the antipodal point. As one would expect, the results differ substantially near the craters, but the distant seismic effects are almost indistinguishable.

We now describe two calculations designed to test the sensitivity of the results to a physical property of the planetary interior, namely the shear strength. In both calculations we consider self-gravitating planets of uniform density ρ , with

$$\rho = \rho_0 = 3.21 \text{ gm/cm}^3.$$

Other relevant material properties common to both calculations are as follows:

$$c_0 = 5.23 \text{ Kilometers/second}$$

$$s = 1.27$$

$$\Gamma_0 = 1.54$$

$$H = 0.2$$

$$Y_o = 600 \text{ bars}$$

$$K_o = \rho_o c_o^2$$

The planetary radius is 2000 kilometers, and the energy deposited (as a buried explosion) is approximately 10^{25} J. We are using Hugoniot data given by van Thiel (1966) for Olivine.

The calculations differ only in the values of the melt energy E_m . Since the temperature increases with depth, we can arbitrarily select a melt energy which will provide a molten interior of any desired radius. For the two calculations, we have chosen, as extreme situations, melt energies which give in one case a completely solid planet, and in the other a planet which, except for a thin solid surface, is completely molten.

Clearly this problem is not intended to represent in detail a realistic model of any specific planetary interior. Nor do we wish to emphasize too strongly the quantitative results of these early calculations. Nevertheless these material properties are not unreasonable for the smaller terrestrial planets, especially if they lack condensed cores at the relevant stage in their histories. Therefore we expect that our results are qualitatively correct, and probably are close order-of-magnitude estimates of the actual physical situation.

Figure (4) shows contour plots of the material density (a good measure of the overall compressive or rarefactive nature of the shock wave) at selected times for both calculations. In both cases a nearly spherical compressive wave is propagated from the impact point, trailed immediately by a broad rarefaction zone. This direct wave arrives at the antipode about ten minutes after impact.

Following this initial signal is a complicated pattern of stresses generated by interactions of the initial wave with the free surface. A prominent feature of this pattern is a second compressive front which converges quite sharply at the antipode (see especially Figure [4f]) about twenty minutes after impact.

Late-time seismic activity deep beneath the antipode is particularly interesting. Between about fifteen and thirty minutes after impact, violent and persistent oscillations in density and stress, showing very steep spatial gradients, are produced by constructive and destructive interference among waves singly- and multiply-reflected from the free surface. Excluding the crater region, the antipode is the scene of the most vigorous surface motion, but the strongest manifestations of these oscillations occur beneath the antipode, at depths as great as half the planetary radius.

Although the results of the two calculations possess qualitative similarities, the seismic response of the molten planet is greater (by factors of two to three) than that of the solid planet. We attribute this difference to the more effective energy dissipation mechanisms present in the solid. In propagating through the solid, a wave must do work to produce shearing deformations; if the wave is strong enough, energy is lost in producing plastic deformations, or in breaking the material. These avenues of energy loss are not available in the purely hydrodynamic calculation describing the molten material. In Figure (5) we show the time histories of the surface displacement, the surface velocity, and

the minimum principal stress near the antipodal point, for both calculations. The velocity and displacement plots show particularly well the greater strength of the seismic effects in the case of the molten planet.

The minimum principal stress is an important quantity in that it is the first stress component to reveal tension (by being negative), and is therefore the indicator for tensile failure. Figures (5e) and (5f) record this stress component at a depth of 33 kilometers beneath the antipode (because that is the depth of the center of the outermost computational cell). For the planet with a molten interior, tensile failure occurs (twice: at 1130 and 1400 seconds) even at that depth, where the ambient hydrostatic pressure is almost two kilobars. For the completely solid planet, tensile failure does not occur at that depth, but a very strong relative rarefaction, about .75 kilobar, is present. It is therefore likely that the surface near the antipode is fractured to a considerable depth, although not as deeply as in the molten case. These strong rarefactions are not confined to the antipode, but with varying strength encounter the surface globally. Our calculations thus raise the intriguing possibility that the seismic effects from sufficiently large impacts may be great enough to fracture the entire surface of the planet.

4. Conclusions

The calculations described in the foregoing section lead us to several general conclusions. We shall list these in the order of decreasing certainty.

- a. The distant seismic effects of impacts and near-surface explosions are similar and are rather insensitive to the detailed manner of the energy release.
- b. Antipodal seismic focusing occurs and appears to be of morphological significance. We find ground motions on the order of kilometers, velocities of tens of meters/second, and accelerations approaching one lunar gravity.
- c. The strongest effects are caused not by direct shock waves, but by the complex interference patterns of waves reflected from the free surface. Furthermore the most dramatic responses are seen at great depths within the planet.
- d. The seismic response of a molten planet is greater than that of a solid one. Thus the presence of interior molten layers at the time of the basin-forming impacts will have a significant influence on the transmission of seismic energy from these impacts.
- e. Tensile failure occurs to considerable depth near the antipode and may occur (to moderate depths) globally. This raises the possibility that the basin-forming impacts may have repeatedly brecciated the entire early lithospheres of each of the terrestrial planets.

Acknowledgments

This research was supported in part by NASA (Planetary Geology Programs Office) and in part by the US-ERDA. We benefited from discussions with Peter Schultz, Sean Solomon, Thomas Weaver, and Eric Jones. Maxwell T. Sandford, II also assisted us in reproducing the computer graphics.

References

- Bertholf, L. D. and Benzley, S. E., 1968. TOODY II: A Computer Program for Two-Dimensional Wave Propagation. Sandia Laboratories Research Report SC-RR-68-41.
- Gault, D. E. and Wedekind, J. A., 1969. The Destruction of Tektites by Micrometeoroid Impact. J. Geophys. Res. 74, pp. 6780-6794.
- Harlow, F. H. and Amsden, A. A., 1971. Fluid Dynamics. Los Alamos Scientific Laboratory Monograph LA-4700.
- Hartmann, W. K. and Wood, C. A., 1971. Moon: Origin and Evolution of Multi-ring Basins. The Moon 3, pp. 3-78.
- Head, J. W., 1974. Orientale Multi-ringed Basin Interiors and Implications for the Petrogenesis of Lunar Highland Samples. The Moon 11, pp. 327-356.
- Head, J. W., Settle, M., and Stein, R. S., 1975. Volume of Material Ejected from Major Lunar Basins and Implications for the Depth of Excavation of Lunar Samples. Proc. Lunar Sci. Conf. 6th, pp. 2805-2829.
- McGetchin, T. R., Settle, M., and Head, J. W., 1973. Radial Thickness Variation in Impact Crater Ejecta: Implications for Lunar Basin Deposits. Earth Planet. Sci. Lett. 20, pp. 226-236.
- O'Keefe, J. D. and Ahrens, T. J., 1975. Shock Effects from a Large Impact on the Moon. Proc. Lunar Sci. Conf. 6th, pp. 2831-2844.
- Pike, R. J., 1974. Ejecta from Large Craters on the Moon: Comments on the Geometric Model of McGetchin et al. Earth Planet. Sci. Lett. 23, 265-274.
- Schultz, P. H., 1972. A Preliminary Morphologic Study of the Lunar Surface. Ph. D. Thesis, University of Texas at Austin, 967 pp.
- . 1974. Moon Morphology. University of Texas Press, Austin, 626 pp.
- Schultz, P. H. and Gault, D. E., 1975a. Seismic Effects from Major Basin Formations on the Moon and Mercury. The Moon 12, pp. 159-177.
- . 1975b. Seismically Induced Modification of Lunar Surface Features. Proc. Lunar Sci. Conf. 6th, pp. 2845-2862.

- Shoemaker, E. M. and Hackman, R. J., 1962. Stratigraphic Basis for a Lunar Time Scale. In: Z. Kopal and Z. K. Mikhailov (Editors), The Moon. Academic Press, London, pp. 289-300.
- Stuart-Alexander, D. E. and Howard, K. A., 1970. Lunar Maria and Circular Basins — A Review. Icarus 12, pp. 440-456.
- Thorne, B. J. and Holdridge, D. B., 1974. The TOOREZ Lagrangian Rezoning Code. Sandia Laboratories Research Report SLA-73-1057.
- van Thiel, M. (Editor), 1966. Compendium of Shock Wave Data, Vol. 2. Lawrence Livermore Laboratory Report UCRL 50108.
- Wilhelms, D. E. and McCauley, J. F., 1971. Geologic Map of the Near Side of the Moon. U.S. Geol. Survey Misc. Geol. Inv. Map I-703.

FIGURE CAPTIONS

Figure 1. The computational mesh.

- a). Logical space. The grid consists of a rectangular array of cells labeled (i,j) . To each vertex is assigned a position vector \vec{r}_{ij} . To each cell are assigned appropriate thermodynamic quantities ρ_{ij} , E_{ij} , etc.
- b). Physical space. The actual geometric shape of the system is revealed when the vertices (i,j) are placed at the positions \vec{r}_{ij} . Here we see the initial configuration of a spherical planet.

Figure 2. The logical path followed in computing the time evolution of the stress field.

Figure 3. Comparison of the shock waves from a simulated impact (a), and a buried explosion (b). In either case the energy ($\approx 10^{24}$ J) is deposited at the right side of the figure, on the symmetry axis. These are contour plots of the second deviatoric stress invariant.

Figure 4. Contour plots of material density at three selected times for a completely solid planet and for a planet with a completely molten interior.

- a). Solid, at 400 seconds. b). Molten, at 400 seconds.
- c). Solid, at 600 seconds. d). Molten, at 600 seconds.
- e). Solid, at 1400 seconds. f). Molten, at 1400 seconds.

In both cases the energy deposited is approximately 10^{25} J; the material properties for these calculations are described in the text. The blank areas in the

cratering regions are not empty, but represent density excursions beyond the scale chosen for the contour plots.

Figure 5. Time histories of surface displacement, surface velocity, and minimum principal stress near the antipode for the two calculations illustrated in Figure 4.

- | | |
|-----------------------------------|------------------------------------|
| a). Displacement, solid planet. | b). Displacement, molten planet. |
| c). Velocity, solid planet. | d). Velocity, molten planet. |
| e). Minimum stress, solid planet. | f). Minimum stress, molten planet. |

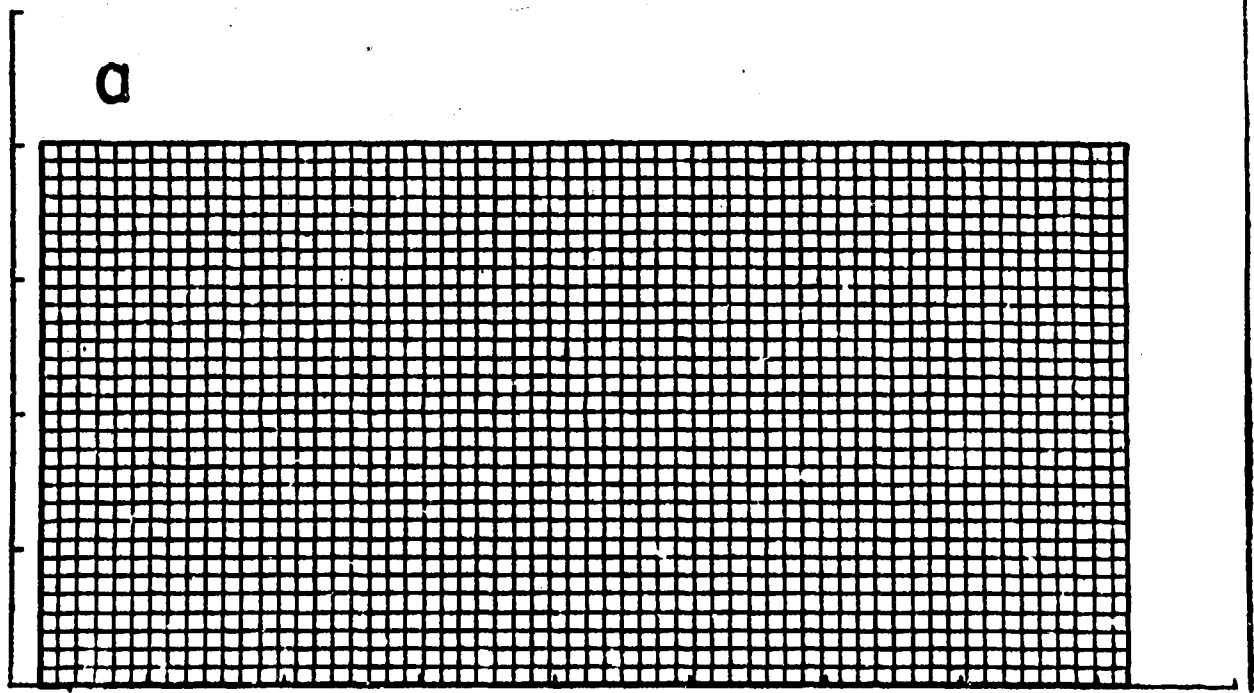


Figure 1a

H. Grady Hughes, et al
Global Seismic Effects
Figure 1a

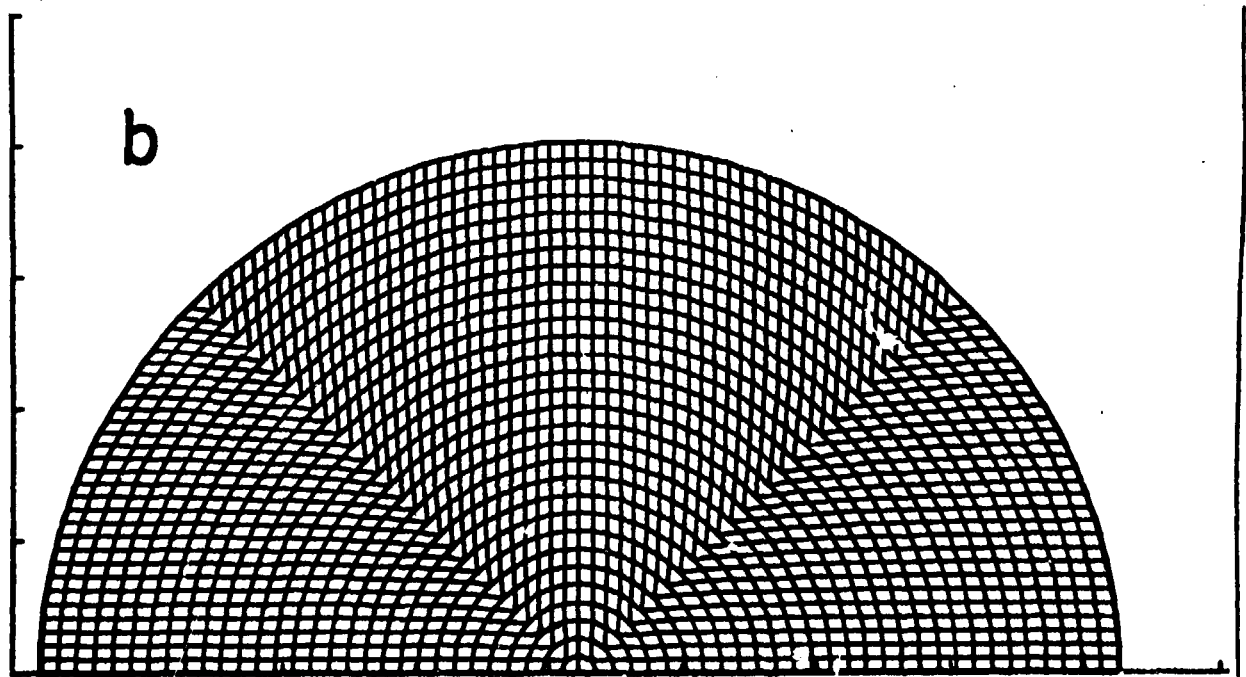


Figure 1b

H. Grady Hughes, et al
Global Seismic Effects
Figure 1b

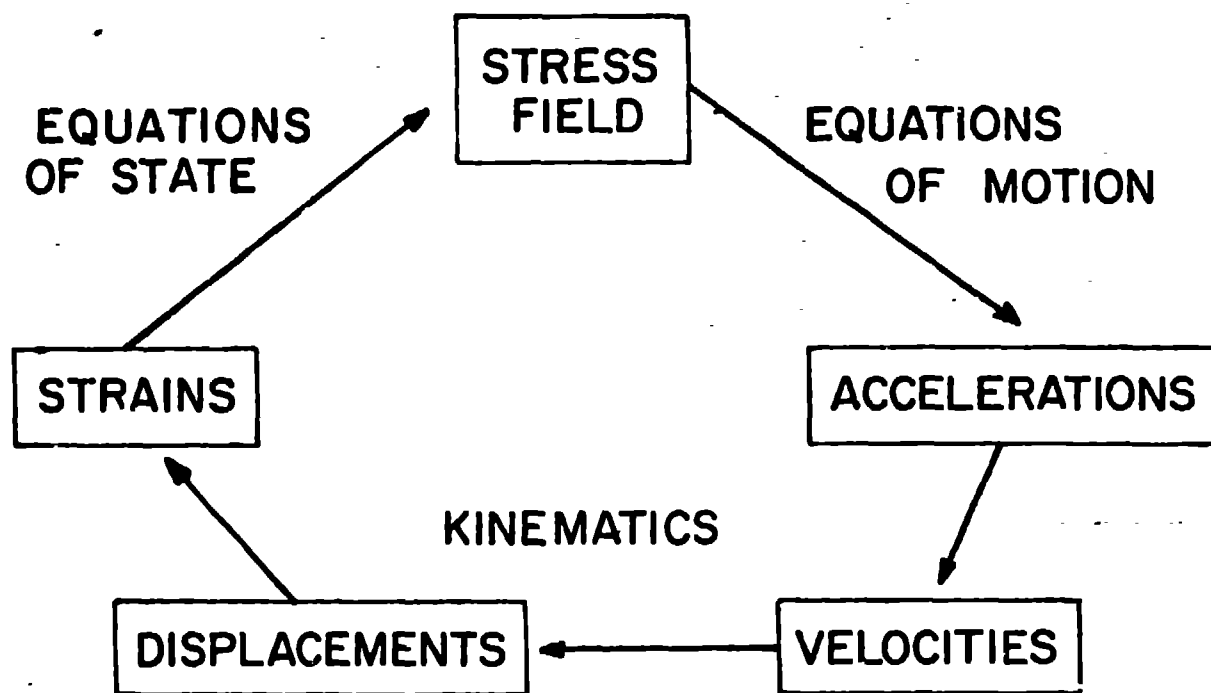


Figure 2.

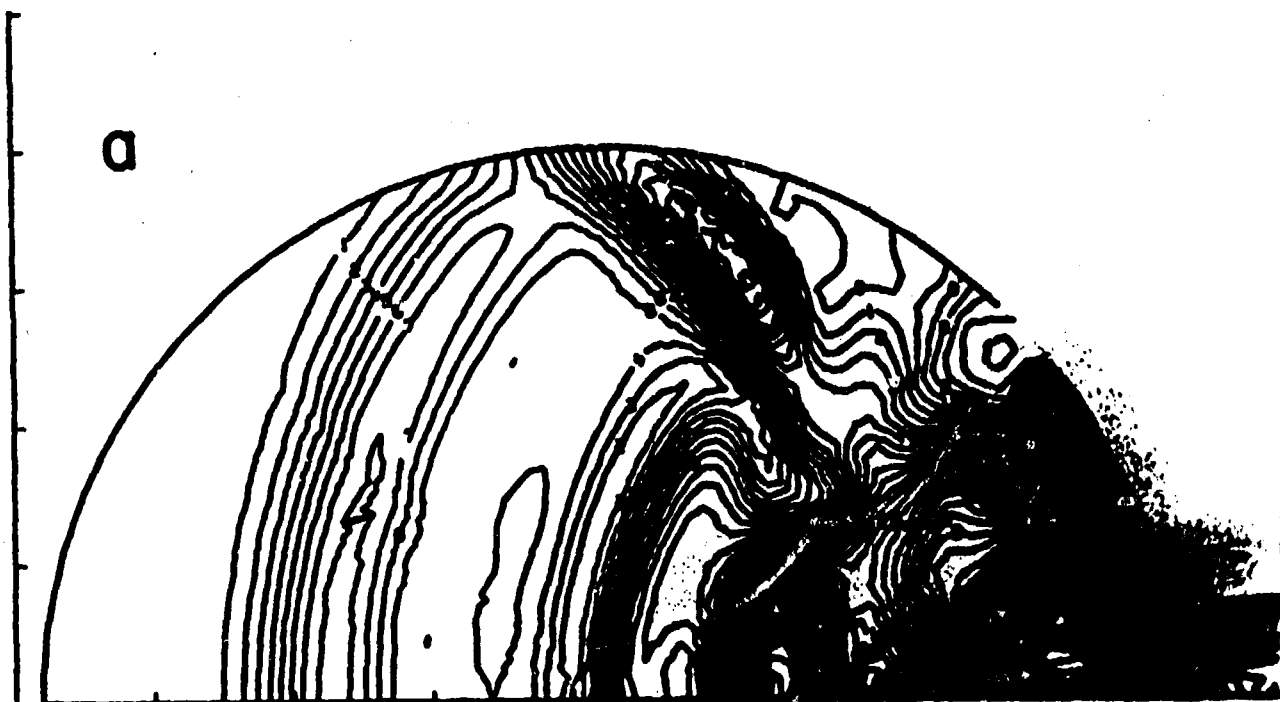


Figure 3a

H. Grady Hughes, et al.
Global Seismic Effects
Figure 3a

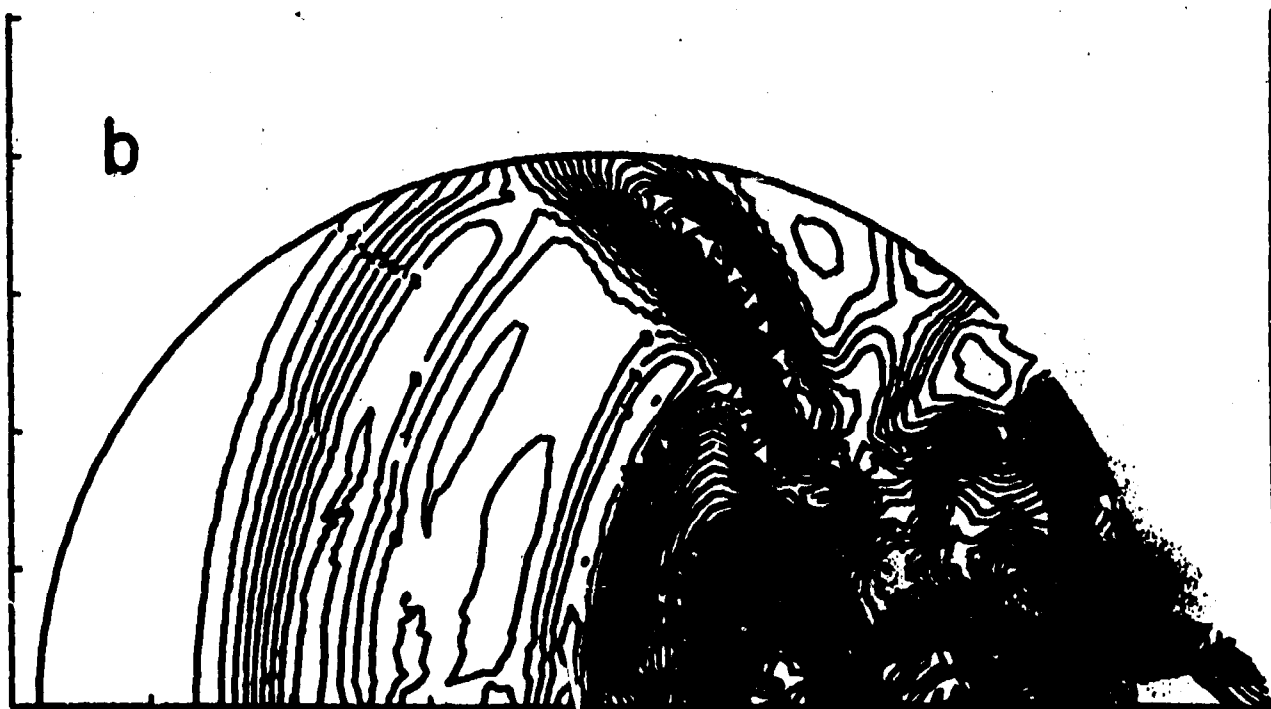


Figure 3b

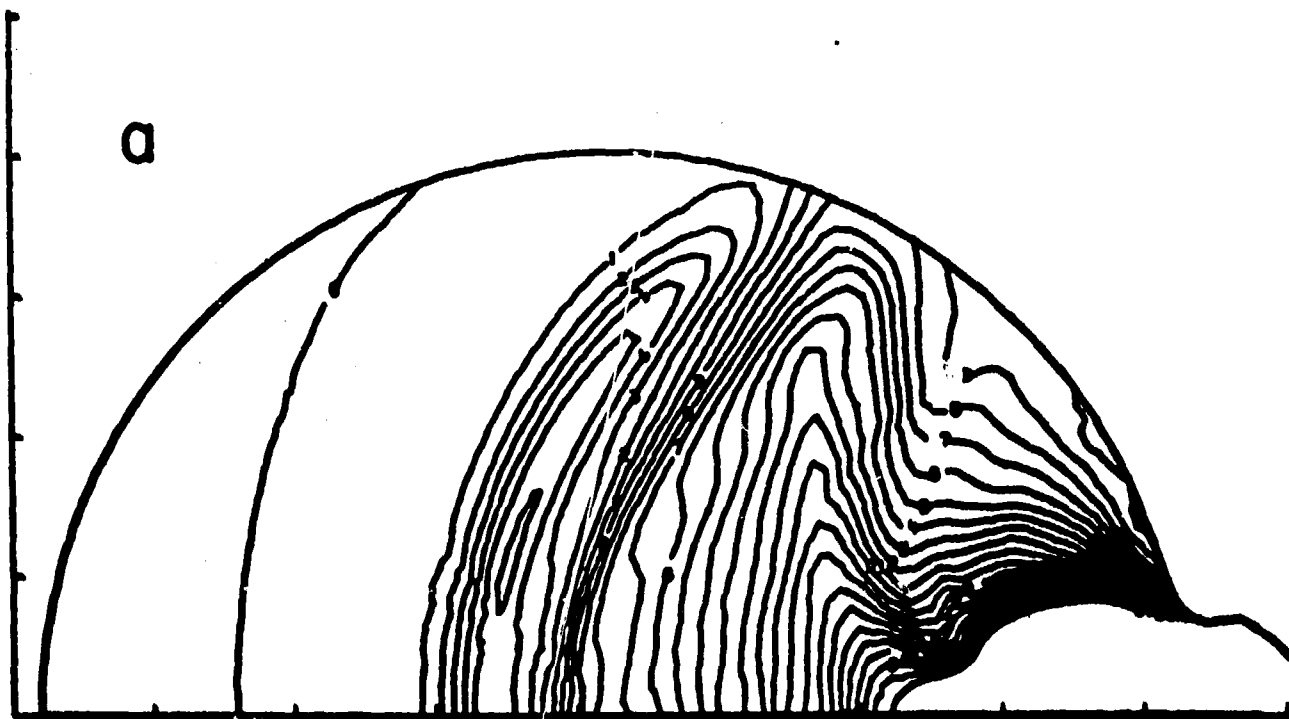


Figure 4a

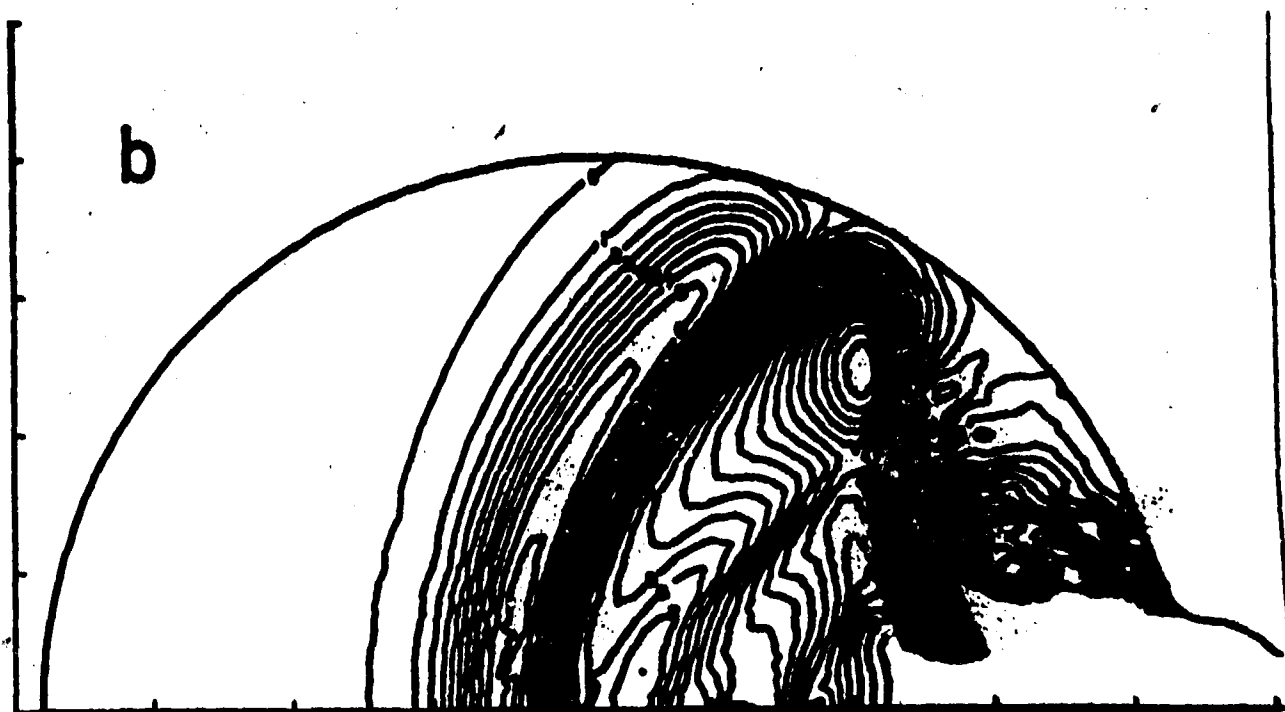


Figure 4b

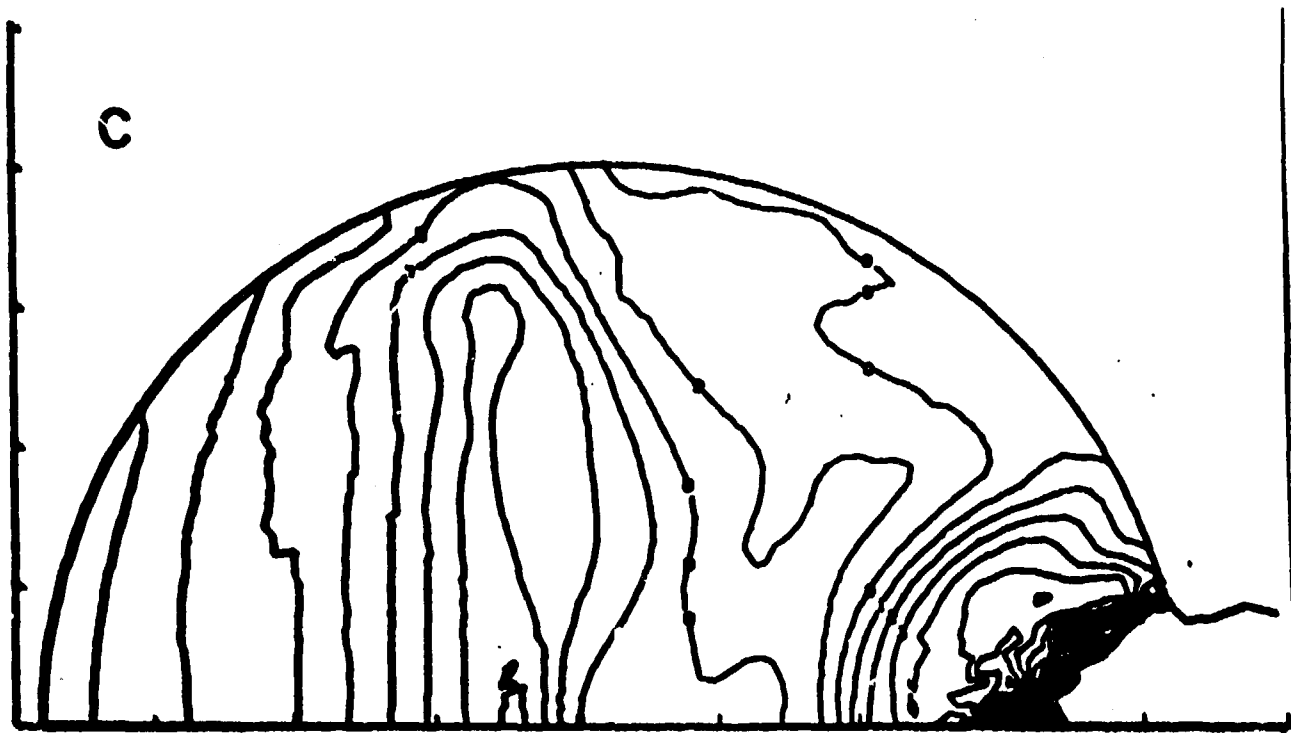


Figure 4c



Figure 4d

H. Grady Hughes, et al
Global Seismic Effects
Figure 4d



Figure 4e

H. Grady Hughes, et al
Global Seismic Effects
Figure 4e

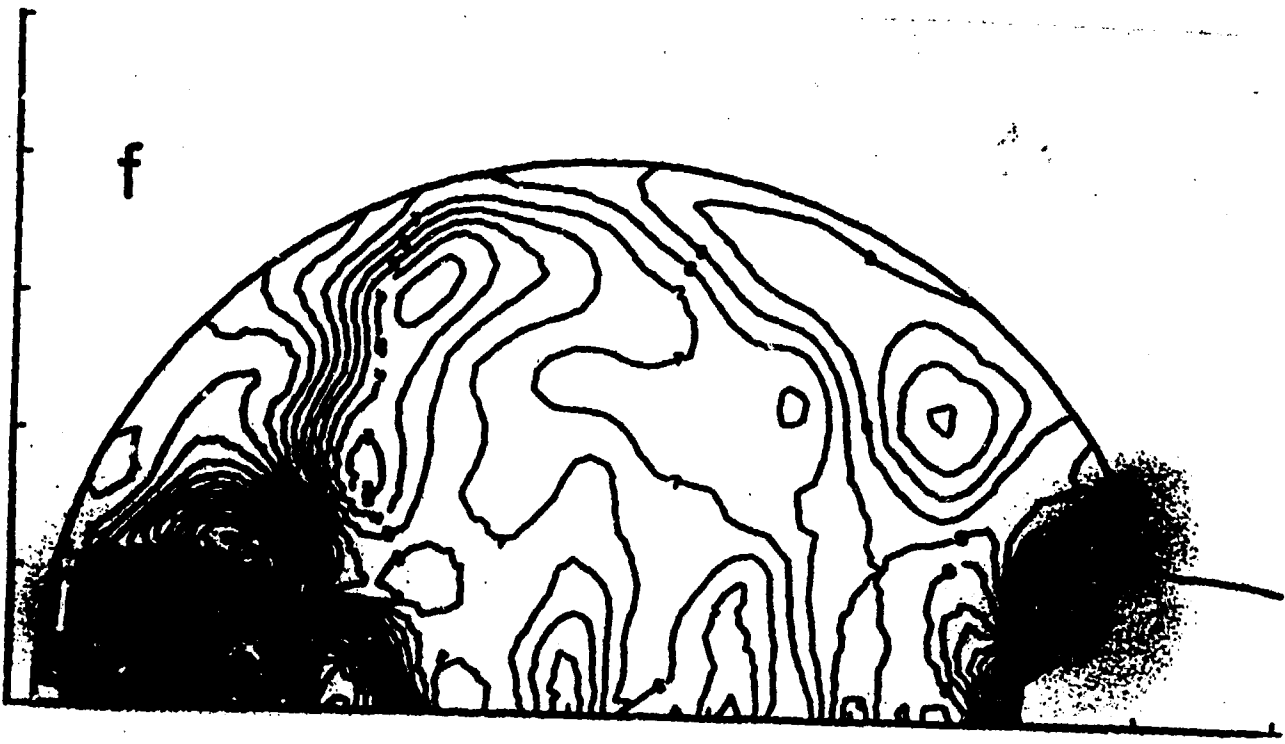


Figure 4f

H. Grady Hughes, et al
Global Seismic Effects
Figure 4f

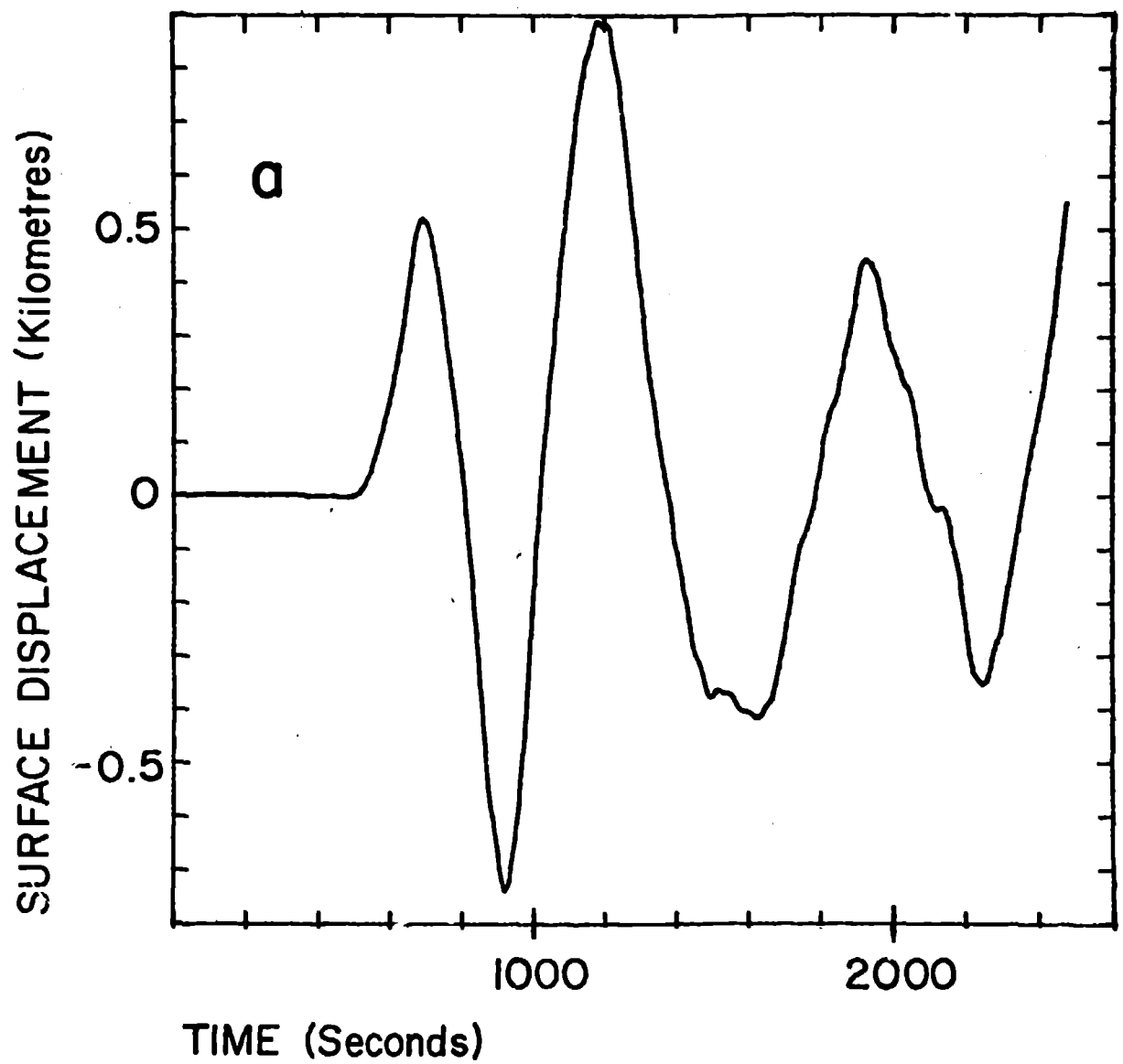


Figure 5a

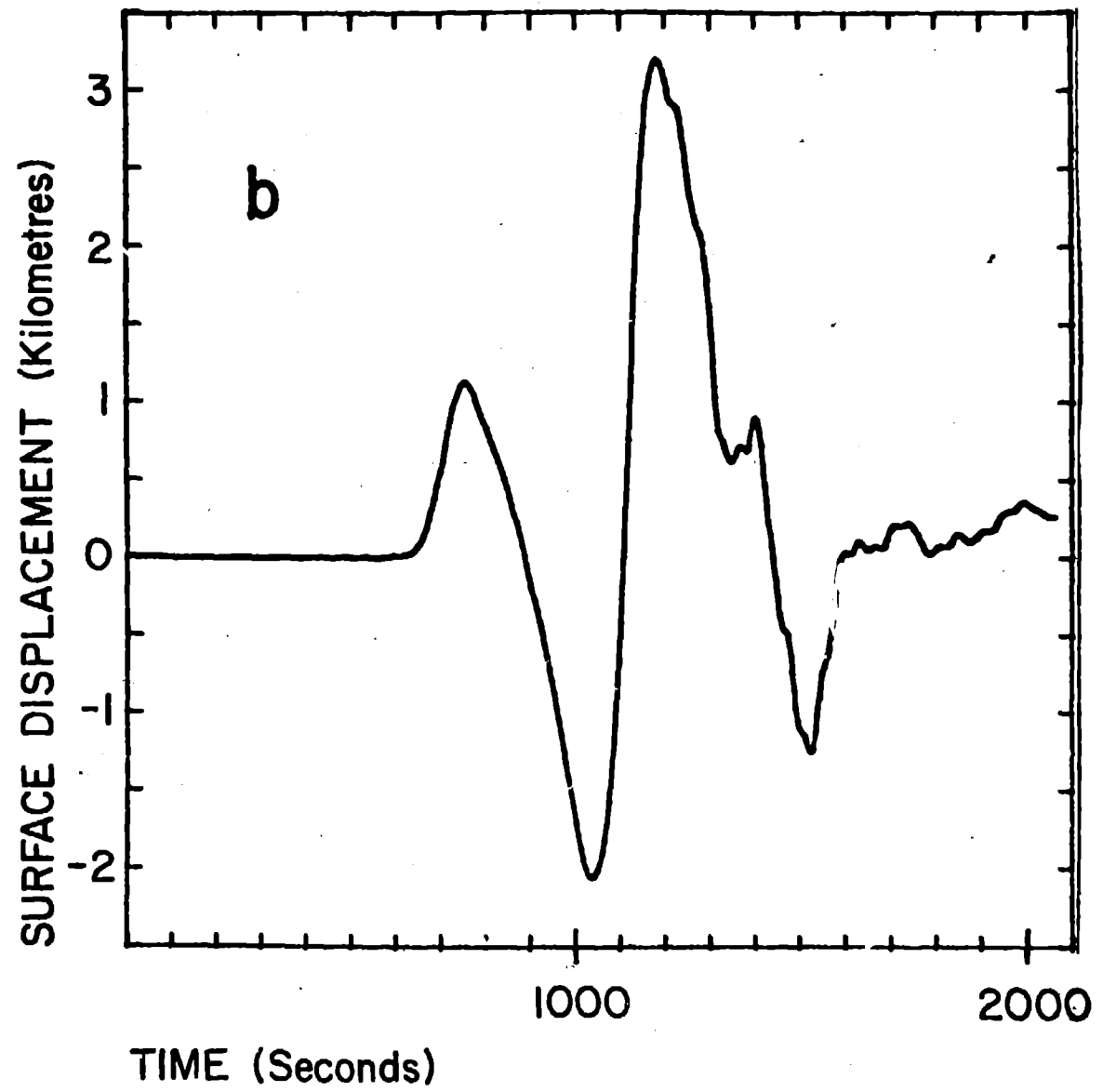


Figure 5b

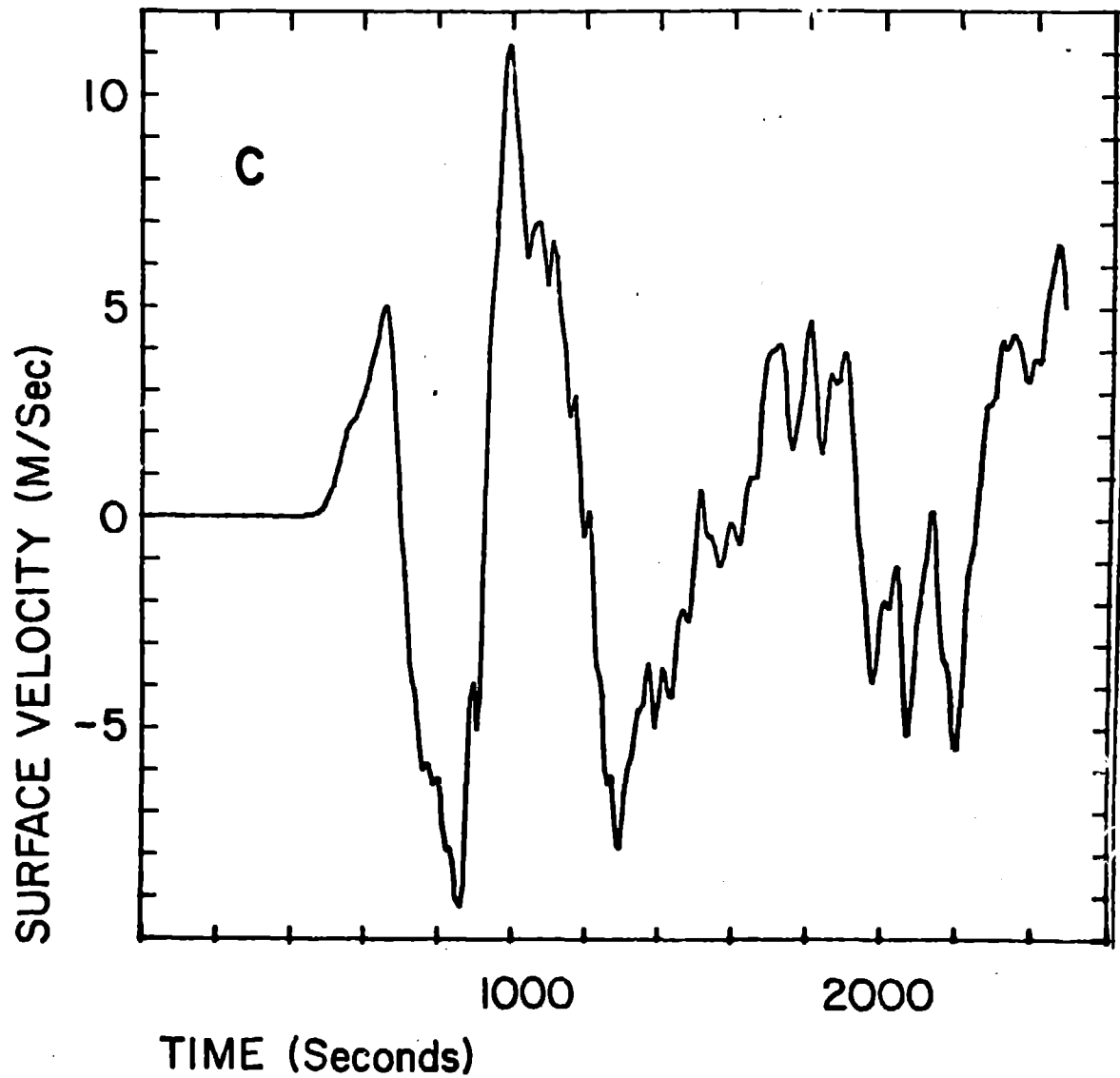


Figure 5c

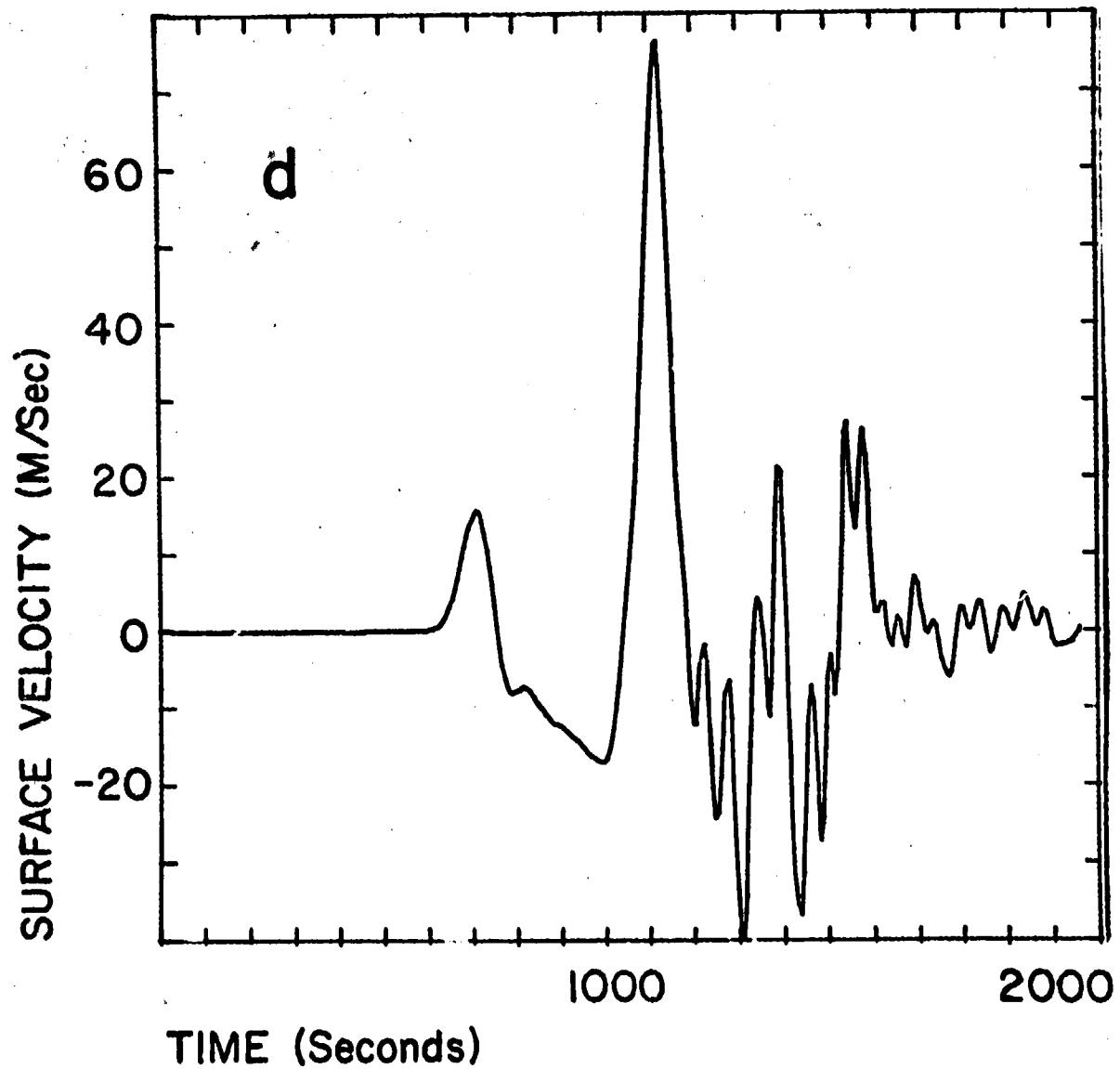


Figure 5d

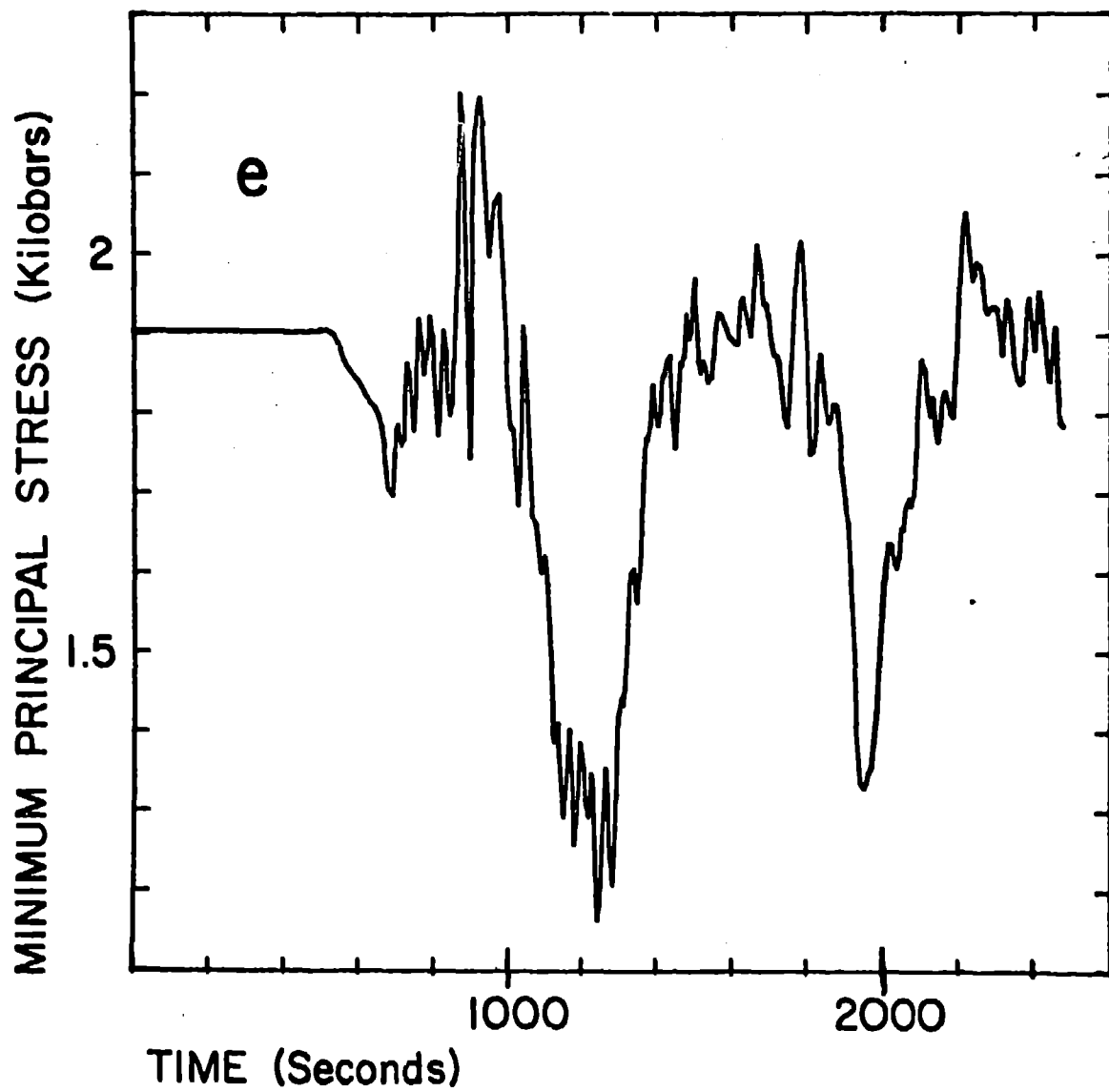


Figure 5e

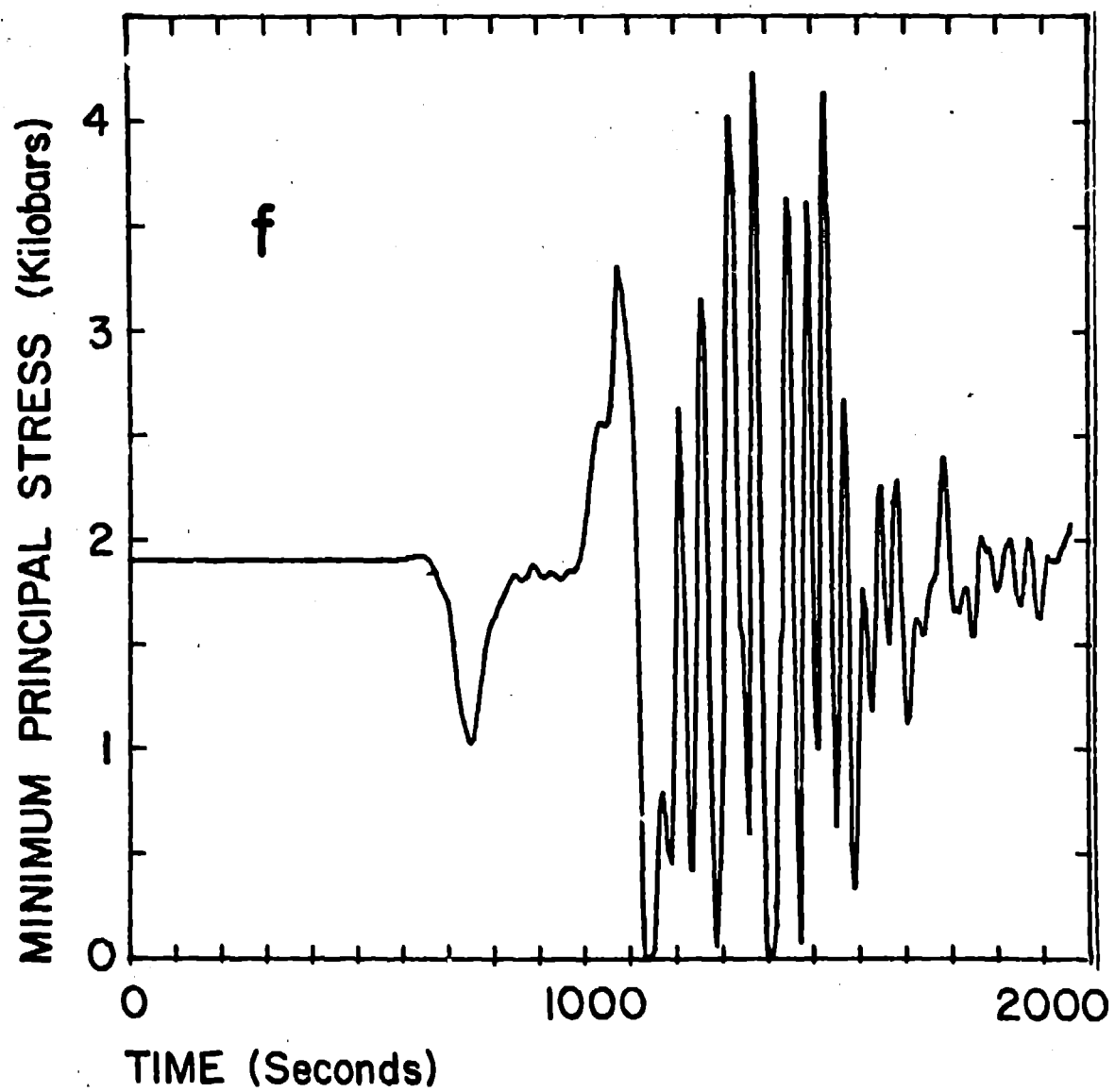


Figure 5f